Surface ionizing dose deposited by low energy electrons (10 eV–10 keV) in eleven monoatomic materials: Monte Carlo calculations and analytical expressions

Quentin Gibaru, Christophe Inguimbert, Pablo Caron, Mohamed Belhaj, Mélanie Raine, Damien Lambert

Surface ionizing dose deposited by low energy electrons (10eV-10keV) in eleven monoatomic materials: Monte Carlo calculations and analytical expressions

Q. Gibaru[1,2,3*], C. Inguimbert[1], P. Caron[1], M. Belhaj[1], M. Raine[2], D. Lambert[2]

[1]ONERA-DPHY, 2 avenue E. Belin, 31055 Toulouse, France
[2]CEA, DAM, DIF - 91297 ARPAJON, France
[3]CNES, 18 av. E. Belin, 31401 Toulouse CEDEX, France
*quentin.gibaru@onera.fr

Abstract

An analytical formula for the ionizing dose of low energy electrons is proposed. The expressions have been validated for 11 monatomic elements (C, Be, Al, Si, Ti, Ni, Cu, Ge, Ag, Fe and W) and for energies ranging from ~10 eV up to 14.5keV by the use of low energy Monte Carlo simulations. These expressions can be used to evaluate the energy loss of low energy electrons as an input for other simulation codes.

1 Introduction

The transportation of low energy electrons in matter and its study is of great interest in many applications such as nuclear physics, medicine and space applications. In the field of space technologies, the estimation of the ionizing dose deposited near the surface of satellites (~10 nm) is a key concern for space missions [1], as the energy received by the materials (Al, Ag, Cu, Si, glasses, polymer coatings…) may cause some degradations and disturb the on-board systems.

In particular, the ionizing dose, which is the quantity of energy deposited per unit of mass of a target material, is a common metric very useful to several fields. For example, many degradations induced by radiations from the space environment are scaled according to the ionizing dose, such as electrical discharges, or the degradation of the optical properties of surface polymer coatings [1]. Some domains related to electron beams, such as electron spectroscopy also benefit from an accurate estimation of the dose. The related secondary electron emission (SEE) process is crucial regarding the efficiency of various devices [2,3], whose materials may be selected to modify the emission rate. For instance, the multipactor electron-cloud effect that happens in Radio-Frequency (RF) components of satellites is driven by the SEE Yield (SEY) [4,5]. As a result, low emissive materials are needed in order to prevent the formation of an electron cloud which can lead to Corona electrical discharges. In this context, the ionizing dose is related to the SEY, and is a fundamental parameter commonly used in SEE yield models [6,7].

Indeed, the energy deposited in the material by the incident electrons is the source of production of the secondary electrons that may escape the material. These electrons escape only from depths of a few nanometers, corresponding to energies down to a few tens of eVs. Consequently, the dose needs to be evaluated for electrons down to very low

energies, and with a nanometric precision, in order to get an accurate estimation of the resulting electron cascade. But this is not the case in general, the ionizing dose being well simulated for electrons having energies higher than some keV and at micrometric scale.

Therefore, the knowledge of empirical formulas providing the dose deposited as a function of the depth of the irradiated material is very useful.

Several empirical formulas are already available in the literature. They can be found in SEY models, most of them having been extrapolated from or fitted to experimental data and derived from a range-energy relationship [6–16]. Above some keV the transport of electrons can be approximated by simple laws that neglect at first order the statistical fluctuation of the transport process. But this approximation becomes invalid at lower energies [17]. Consequently, the validity of the expressions based on a constant energy loss or power law extends at best down to ~1 keV, even though they are used for the SEY of electrons of a few hundred eVs. In this case, fitting factors generally have to be included in the SEY model to compensate for this approximation. But several applications, such as secondary electron emission or surface analysis, would benefit from improved models which accurately describe the transport of low energy electrons down to a few eVs.

This is what we did in a previous paper [17]. The Monte Carlo electron transport code MicroElec [18–20], a module of GEANT4 [21], has been used for 11 materials as a reference to extend the validity domain of the range/energy and transmission probability expressions proposed by Kobetich & Katz [10,11]. The improved formula ranges from a few tens of eV up to several tens of MeV [17].

Within this scope, we propose here to carry on with this work and determine numerically the ionizing dose of electrons down to a few tens of eVs. In this paper, we propose an analytical expression for the dose-depth profile of low energy electrons. This expression uses our analytical model for the range and transmission rate of electrons [17]. Our approach was to follow the physics of the transport of low energy electrons, to derive analytical expressions for the dose profiles. This approach allows the model to faithfully reproduce the dose-depth profiles given by Monte-Carlo simulations, with a validity spanning from a few tens of eVs up to 14.5 keV, while, above this energy former expressions can profitably be used [10, 11].

2 Monte-Carlo code for low energy electrons

Monte-Carlo simulation codes have been widely used to compute the secondary electron emission of various materials under electron irradiation, including metals [22,23] or insulators [24,25], or under ion irradiation [26]. In this work, we use the MicroElec module [18–20] of the toolkit GEANT4 for Monte-Carlo simulation. The code can handle the transport of low energy electrons down to a few eV for 11 materials, and has been validated for this purpose using experimental SEY data.

In the [eV - keV] energy range, electrons can be elastically scattered by the nuclei or inelastically scattered by the electrons. In this case, the main source of energy loss for the incident electrons are inelastic interactions with weakly bound and plasmon electrons.

The cross sections for the inelastic interaction can be obtained with the complex dielectric function theory. MicroElec uses this formalism, with the Mermin dielectric function model being used to fit experimental OELF data, following an approach also found in other Monte-Carlo codes such as Denton et al. [27] or Da et al. [28]. A detailed description of the code is available in reference [20].

The dielectric function formalism is used in MicroElec for all types of inelastic interactions, namely plasmons, interband transitions and core shells. Finally, the elastic cross sections

are obtained from the ELSEPA code [29] and the partial wave method, and the surface barrier is modelled with its associated height and crossing probability.

MicroElec can be used to compute the SEY of several materials. In the newly released version of MicroElec (GEANT4 10.7), the transportation of low energy electrons can be simulated in C, Al, Si, Ti, Ni, Cu, Ge, Ag, W, SiO_2 and Kapton. SEY simulations can also be done on Be, Fe and Au, these materials should be available in a future release of GEANT4. The experimental validation for these 3 new materials is shown in this paper below. For the other 11 materials currently available in GEANT4 10.7, the validation can be found in [20].

The SEY of materials is driven by several factors. The inelastic mean free path and differential cross sections control the number of secondary electrons, which can be set into motion by a primary particle, as well as their energy distribution. The elastic Mean Free Path (MFP) has a strong influence on the penetration and escape depth of low energy electrons in the material, as the associated angular deviations make these electrons highly scattered. Finally, the surface potential barrier is associated with a transmission probability which limits the quantity of low energy electrons escaping from the material. As a result, the SEY is an interesting quantity that depends on the combination of all the electron-matter interactions handled in MicroElec. SEYs are also available from experimental measurements, and the comparison between the MicroElec SEY and the experimental data can be used as a validation of the code.

In Figure 1, the SEYs for the 3 new materials are compared with experimental data from Bronstein [30] and multiple SEY datasets from the database of Joy [31], to take into account the possible dispersion between different SEY measurements for a single material. All the simulations have been performed considering in the case of a normal incidence beam on a flat semi-infinite surface, to match the experimental conditions. Overall, the SEYs are in a satisfactory agreement with the experimental data (average error for Be: 23%, Fe: 15%, Au: 9%), considering the spread between the different datasets for the materials, and assuming that the samples have the least possible amount of surface contamination.

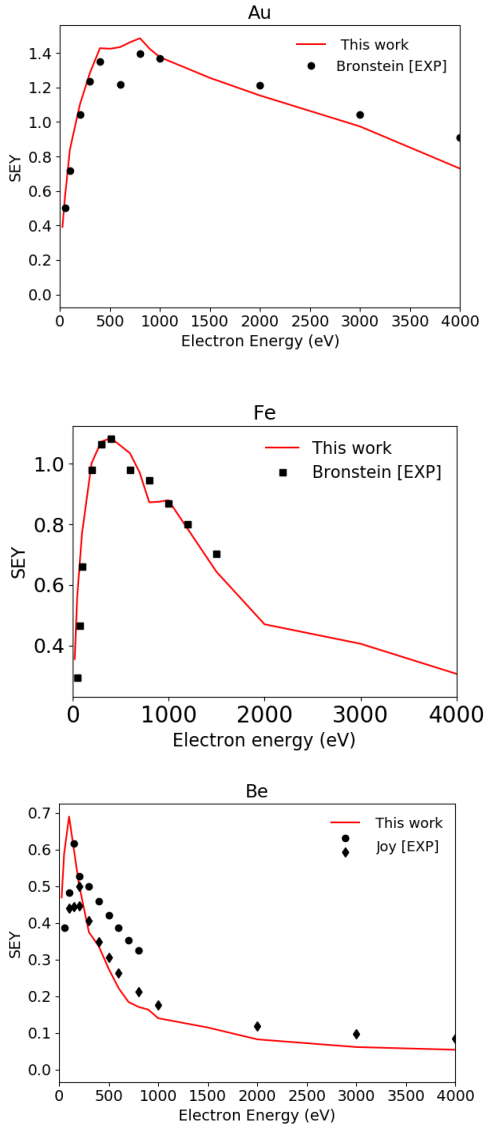

Figure 1: SEYs of Be, Au and Fe computed with MicroElec and compared to experimental data from Bronstein [30] (Fe, Au), and 2 SEY datasets from the database of Joy [31] (Be)

Another metric which has been used to validate the code are the stopping powers,

which are deduced from the inelastic cross sections σ by the relation

$$S(E) = N \int_0^{E_{max}} \hbar\omega \frac{d\sigma}{d(\hbar\omega)}(E, \hbar\omega) d(\hbar\omega)$$

(1)

Where N is the density of atoms per cm^3. As a result, the stopping powers can be used to check the validity of the inelastic mean free paths and the modeling of the OELF. The stopping powers of electrons in the 3 materials are shown below, and compared with calculated data from Shinotsuka et al. [32] and ESTAR [33]. Experimental stopping power data from Joy's database [31] for Au is also added.

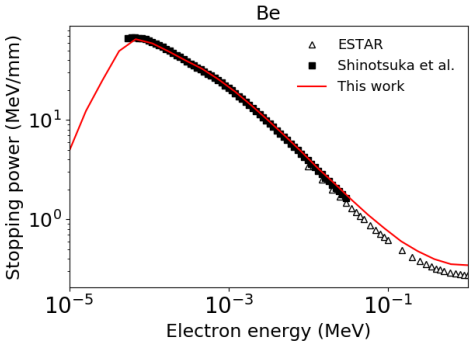

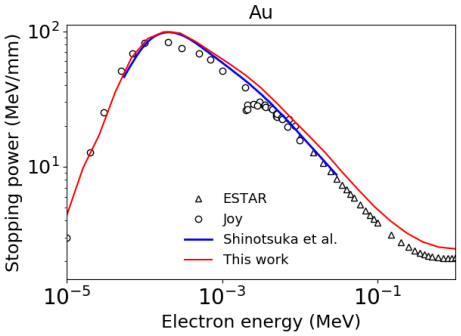

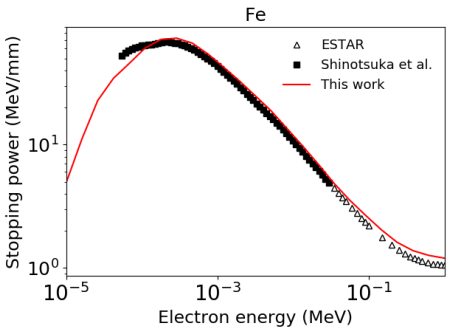

Figure 2: Stopping powers of Be, Au and Fe from MicroElec and compared to data from the literature

As can be seen in Figure 2, the stopping powers computed for these materials are also satisfactorily consistent with the data from the literature, as is the case of the stopping powers of the other 11 materials which can be found in [20]. The average error between MicroElec and the reference data is 10.3% for Be, 11.4% for Fe and for Au.

The models used in MicroElec have been validated by Inguimbert et al. [1] for the calculation of ionizing doses for low energy electrons. In particular, a discrepancy with the standard physics of GEANT4 has been shown. The simulation results of MicroElec have also been used to extend the validity of the analytical formula proposed by Kobetich & Katz [11] for the extrapolated range and transmission probabilities of electrons, down to a few tens of eVs in monoatomic materials. In this study, we propose to use MicroElec as a reference to compute the ionizing dose of low energy electrons in 11 monoatomic materials, and use the simulated data with our improved range-energy expression to calibrate an analytical model for the dose-depth profile of low energy electrons.

3 Analytical model for the dose of low energy electrons

3.1 General expression for the dose-depth profile

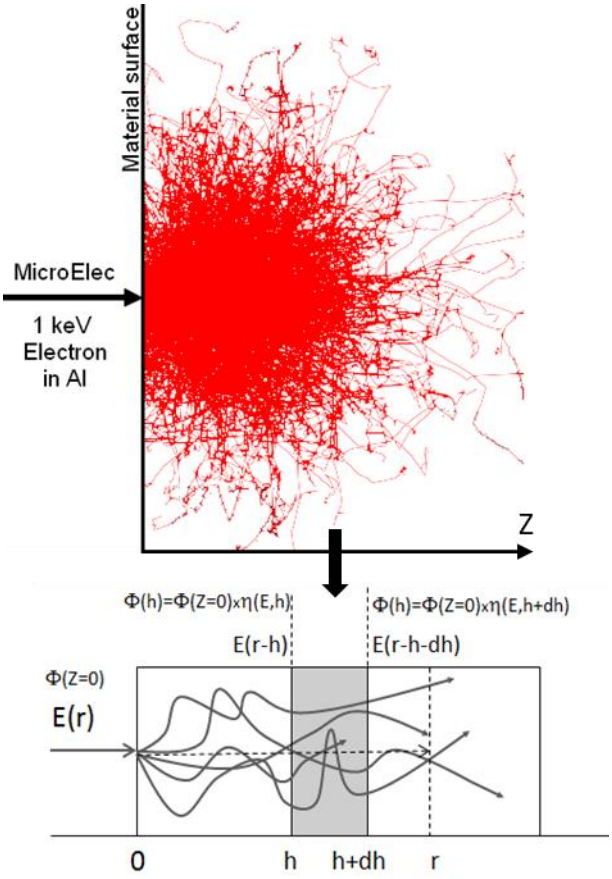

Figure 3: Definition of the energy deposited in a layer of thickness dh at a depth h by an incident fluence of particles of energy E.

The dose is the average energy transferred to the electrons of the medium consecutively to inelastic electron/electron interactions. It corresponds to the average energy deposited by unit of mass of the target material thanks to ionizing interactions. The number of secondary electrons set into motion in the medium is proportional to this physical quantity.

Let us calculate the dose deposited in a layer of thickness *dh*, located at the depth *h* of a material irradiated with a fluence ϕ of incident electrons having an energy *E*. The amount of energy *dE* deposited in this layer of thickness *dh* is given by the subtraction from the amount of energy arriving at the depth *h* of the amount of energy leaving the volume at the depth *h+dh*. The amount of energy transported at the depth *h* is also proportional to the transmitted fluence $\phi \times \eta(h,E)$, $\eta(h,E)$ being the transmission probability of the electrons of energy *E* through a material of thickness *h*. It is also proportional to the energy of the particle at the depth *h* (*E(r-h)*), *r-h* being the remaining distance that the particle of energy *E* has to travel after having previously travelled the distance *h* in the medium :

$$\varphi \cdot \eta(h,E) \cdot E(r-h)$$

(2)

Similarly, the amount of remaining energy at the depth h+dh is given by :

$$\varphi \cdot \eta(h+dh,E) \cdot E\big(r-(h+dh)\big)$$

(3)

The substraction of these two terms leads to the expression of the dose deposited at the depth *h*:

$$dose \propto \varphi \frac{d[\eta(h,E) \cdot E(r-h)]}{dh}$$

(4)

What is noticeable here is that the dose is, for electrons of energy *E*, a simple function of both the transmission probability η(h,E), and the practical range vs. energy expressions r(E) (explicitly E(r-h) in formula (4)) of these electrons..

Many analytical expressions have been proposed for the transmission probabilities and extrapolated ranges of electrons [11,9,10,34–40]. However, the expressions found at higher energies (> keV) are based on the fact that the number of interactions by unit path length is large. At lower energies the inelastic mean free paths reaches values of the order of the distance that can be travelled by the particles while the probability that elastic interactions occur is increasing. The models developed for high energies (> keV)

fail at very low energy and the formula established at higher energies, in the form of a power law relationship, becomes invalid below 1 keV. In our previous work [17], we have extended the work of Kobetich and Katz [10,11], which is based on the expressions proposed by Weber [9]. These expressions have been made applicable for low energy electrons, down to a few tens of eVs. These analytical expressions (reminded below) will be used in this work to propose an analytical formula for the dose profile of low energy electrons.

The range-energy relationship $r(E)$ is given by:

$10eV < E \leq 14.5keV: r(E) = D(E + E_r)^F$ (5a)

$E \geq 14.5keV: r(E) = AE\left[1 - \frac{B}{(1+CE)}\right]$ (5b)

Above 14.5 keV the original expression of ref.[11] is retained (eq 5b), since it is able to faithfully reproduce the extrapolated range.

The transmission probability is inferred from $r(E)$ by the following relationship:

$\eta(E,h) = e^{-\left(\frac{qh}{r(E)}\right)^p}$ (6)

The different parameters of the model (A, B, C, D, E_r, F, G) are provided in ref. [17] and reminded in Appendix I. They are specific to each material and have been tabulated for 11 different materials thanks to the Monte Carlo simulations. The parameters A, B and C are from Weber's formula and depend on the atomic number Z of the material. F and G are defined per material and are provided in ref. [17] for the 11 materials studied here. The parameters D and E_r depend on the other parameters A, B, C, F and G. E_r is a constant in the form of an energy, it is defined by the value of the range below 100 eV but also constrained by the connection between the equations 5a and 5b at 14.5 keV. The connection between the two models is defined such that the values given by the two expressions at 14.5 keV are equal, as well as the derivatives of the two expressions at 14.5 keV.

3.2 Analytical formulas for the dose-depth profile

For higher energies, above 14.5 keV, eq. 5b can be used to calculate the ionizing dose leading to a different formula. This high energy relationship is shown in equation 14 of section 4.2 and compared to the low energy model presented below.

Under some keV, the domain of energy of interest for secondary electron emission and surface analysis, the dose-depth profile can be directly derived from equations (4), (5a) and (6). This gives the expression for the dose:

$$Dose_E(h) = \frac{d}{dh}\left(\eta_E \cdot E(r_E - h)\right) = I'_E(h)\eta_E(h) - I_E(h)\eta'_E(h) \quad (7)$$

Where $\eta_E(h)$ is given by eq. 6.

$I_E(h) = E(r_E - h)$ is the inverse function of the range expression of eq. 5a:

$$I_E(h) = E(r_E - h) = \left[\left(\frac{r_E - h}{D}\right)^{\frac{1}{F}} - E_r\right] \quad (8)$$

The expressions of the derivatives $I'_E(h)$ and $\eta'_E(h)$ can be written as follows:

$$I'_E(h) = \frac{dE(r_E - h)}{dh} = \left[\frac{(r_E - h)^{\frac{1}{F}-1}}{FD^{1/F}}\right] \quad (9)$$

$$\eta'_E(h) = \frac{d\eta_E(h)}{dh} = -\frac{pq}{r_E}\left(\frac{qh}{r_E}\right)^{p-1} e^{\left(-\frac{qh}{r_E}\right)^p} \quad (10)$$

Combining all these expressions lead to a pure analytical expression for the dose vs. depth function. But this initial expression (equation 7 combined with 8-10) is found to slightly underestimate the dose near the surface. Indeed, we have assumed that all primary electrons can only travel forward into the

material. However, a part of the primary electrons can be inelastically backscattered, and leave the material. These electrons will only transfer a part of their energy to the material before exiting it, this energy being deposited near the surface. Another part of the incident fluence can also be elastically backscattered, in which case the electrons will not lose energy in the material. As a result, some corrections have been brought to eq. 7 to take into account these effects and better fit the dose-depth profiles.

For a given depth h, a retrodiffusion factor ζ_{Retro} has been added to reduce the energy deposited by the electrons moving forward into the material. The removed part is compensated by the energy deposited at the depth h by the electrons reflected from deeper into the material, which are traveling back to the surface. The effect of this factor is to redistribute the dose towards the surface and simulate the electrons which have escaped the material but deposited a significant part of their initial energy. The expression (7) becomes:

$$Dose(h) = I'_E(h)\eta_E(h) - \left[(1-\zeta_{Retro})I_E(h)\eta'_E(h) + \zeta_{Retro}\int_h^{r_E} I_E(z)\eta'_E(z)\,dz\right] \quad (11)$$

The retrodiffusion factor has been chosen as $\zeta_{Retro} = 0.1$.

At very low energy, around some tens of eV, the equation (11) does not apply anymore because the transport regime changes to a kind of random walk motion governed by the elastic process that becomes dominant. Indeed, the inelastic mean free path starts to increase very significantly at energies close to the plasmon energy. Equation (11) overestimates the deposited energy, which can become higher than the incident energy. To correct that, below a cutoff energy chosen equal to the plasmon energy of the target material, the ionizing dose have been simplified, following $dE = \varphi \cdot E.\frac{d\eta\cdot}{dh}$. And the dose-depth profile is simplified to:

$$Dose_E(h) = -E \cdot \eta'_E(h) \quad if \quad E \leq \hbar\omega_p \quad (12)$$

This formula avoids any overestimation of the deposited dose at very low energy (E< $\hbar\omega_p$).

In the intermediate energy range [$\hbar\omega_p$, ~300eV], in order to connect smoothly both expressions (11) & (12), a linear combination of these two formula is proposed:

$$Dose_E(h) = \left[\frac{E-\hbar\omega_p}{E_{Low}-\hbar\omega_p}\right] I'_E(h)\eta_E(h) - \left[E\frac{E_{Low}-E}{E_{Low}-\hbar\omega_p} + I_E(h)\frac{E-\hbar\omega_p}{E_{Low}-\hbar\omega_p}\right]\eta'_E(h) \quad (13)$$

Where $E_{Low} = E_r/2$, the definition of E_r is given in Appendix I. E_r is a parameter extracted from the range-energy model in ref. [17]. This expression can be used in the energy range ($\hbar\omega_p$ <E < $E_r/2$). Depending on target material, $E_r/2$ corresponds to energies of a few hundreds of eV.

The deposited energy expression given in (eq. 7) is defined for any electrons entering a target solid. But a part of an incident beam is elastically backscattered limiting the number of entering electrons. The deposited dose which is equal to the product of the incident fluency by the energy loss must be reduced from the amount of reflected electrons.

The proportion of incident electrons entering the irradiated material is equal to $1 - BEY_E$, BEY_E being the amount of elastically backscattered electrons (or Backscattered Electron Yield) for an incident energy E. To summarize, the contribution of the elastically backscattered electrons for a given energy must be removed from the three relationships

for $Dose_E(h)$ (Eqs. 11-13) by removing the BEY. The dose-depth profile is thus obtained by the final expression:

$$Dose = Dose_E(h) * (1 - BEY_E)$$

In this work, we propose an expression for the BEY depending on the material and the incident electrons' energy. It is based on data from MicroElec Monte-Carlo simulations, where we have computed the proportion of backscattered electrons. The BEY is modeled by two single values for low and high energies, which are linearly connected in the intermediate region. The values of the BEY for materials with Z <= 22 on the whole energy range follow the computed values for the true BEY, which is the ratio of primary electrons exiting the material (elastically and inelastically backscattered).

For materials with Z > 22 however, we have to reduce the BEY value used in the model at higher energies to get a better agreement with the Monte-Carlo simulations. In this case, we have used the BEY only computed with the part of incident electrons that are elastically backscattered. We can suppose that for higher Z materials, the backscattered electrons are able to travel deeper into the material and lose more energy. This effect is only partially included in the model, by the use of the factor ζ_{Retro} in eq. 11. Consequently, this modification of the BEY is required to reproduce the Monte-Carlo simulations, which compute the full backscattering process for the incident electrons.

The BEY values with their domain of validity are given in Table 1 below. Between the low energy and high energy values, a linear fit is applied. For W, a unique value has been used.

As can be seen in Table 1, the dose model proposed in this work has only been validated for monoatomic materials, since the transmission probabilities and range expressions are functions of the atomic number of the material.

4 Validation of the analytical model

4.1 Comparison of the analytical model with Monte-Carlo data

The dose-depth profiles, calculated with this model, are compared with Monte Carlo simulation results from MicroElec, in an aluminum target for energies ranging from 10 eV up to 2000 eV. To get these dose profiles, only the primary electrons have been simulated. The secondary electrons, which would have been created from the energy deposited by the incident electrons, have not been generated in the simulation. As the resulting electronic cascade is not simulated, the dose is independent of the SEY. This allows us to get the dose-depth profile per incident electron fluence. Indeed, the elastically and inelastically backscattered electrons are also simulated, and their contribution is thus included in the dose. 50 000 incident electrons have been simulated for each energy, with a computation time of about 1 min per energy.

As can be seen in Figure 4 the analytical model is also in quite good agreement with the Monte Carlo simulation of Walker [41] (9%) at 2 keV. The dispersion between the data of Walker, OSMOSEE [42], MicroElec and the analytical model is higher at 500 eV (25%) than 2 keV (11%), which can be attributed to a

Table 1: BEY values

Material		C	Be Al Si Ti	Fe Ni Cu Ge Ag	W
Z		6	4 13 14 22	26 28 29 32 47	74
Low energy BEY	**Value**	0.1	0.3	0.35	0.35
	Energy domain	E < 21 eV	E < 200 eV	E < 400 eV	
High energy BEY	**Value**	0.02	0.225	0.14	
	Energy domain	E > 700 eV	E > 2 keV	E > 3 keV	

difference in the mean free paths used by the different Monte Carlo codes. Indeed, the authors of ref. [41] indicate that the dose is given by primary electron without considering the effect of the secondary electron cascade, in the same way as MicroElec.

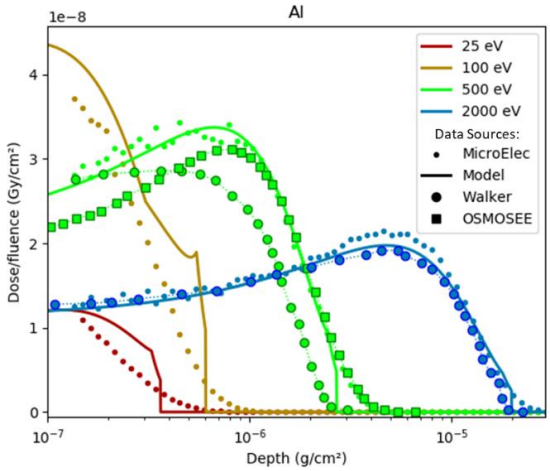

Figure 4. Dose-depth curve given by the analytical model (Model) proposed in this work for incident electrons in aluminum. The model is compared with Monte Carlo simulations of MicroElec, Walker [41] and OSMOSEE [42]. Small circles of different colors are for MicroElec simulations, big circles of different colors are for Walker [36] reference data and different squares are our former simulations performed with OSMOSEE code [37].

Our Monte-Carlo reference code (MicroElec) can be compared with the other electromagnetic physics modules of GEANT4. In figure 5, the dose profiles of electrons in Si given by MicroElec and GRAS [38] are plotted.

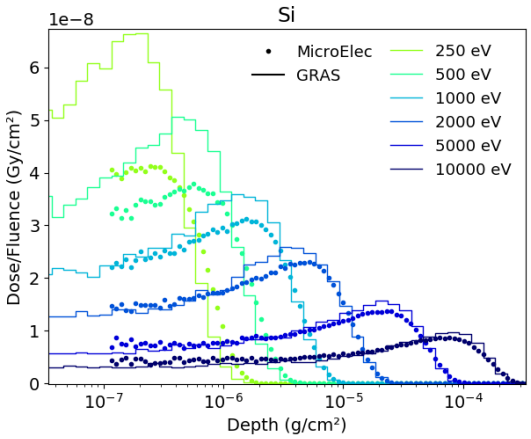

Figure 5: Comparison of the dose profiles in Si from MicroElec and GRAS

GRAS [43] is based on the Geant4 standard electromagnetic physics, which are continuous processes with a condensed history and multiple scattering approach. MicroElec however uses discrete processes, which are slower but more precise at low energies where the step lengths become nanometric. At 2 keV and above, both models give similar dose profiles. Below 1 keV, the electron energy gets closer to the low energy limit of GRAS, and the dose below a depth of 2E-6 g/cm² given by GRAS is much higher than MicroElec. MicroElec is able to give the dose profiles of electrons down to a few eVs, which is an improvement over the low energy limit of GRAS (250 eV). The comparison between MicroElec and GRAS for the other materials studied in this work can be found in Appendix III, and a more detailed comparison between MicroElec and other GEANT4 models can be found in ref. [1]. MicroElec has been chosen as the reference for the analytical dose model due to its ability to transport electrons below 250 eV down to a few eVs. This transport has been validated with experimental SEY data in ref. [20].

4.2 Comparison between the low and high energy models

The high energy model proposed in ref. [11], which includes the range expression given by eq. 5b, can be used to calculate the ionizing dose leading to a formula different from eq. 11. In the same way as in the low energy model (section 3.2), the ionizing dose in the high energy model can be expressed as:

$$Dose_E(h) = \frac{d}{dh}\left(\eta_E \cdot E(r_E - h)\right) = I'_E(h)\eta_E(h) - I_E(h)\eta'_E(h)$$

(14)

Where $r_E = AE\left[1 - \frac{B}{(1+CE)}\right]$ is the high energy range expression from eq. 5b. This gives the inverse range function $I_E(h)$:

$$I_E(h) = E(r_E - h) = \frac{1}{2AC}\left[(r_E - h)C - A(1-B) + \sqrt{\Delta(r_E - h)}\right]$$

And its derivative

$$I'_E(h) = \frac{dE(r_E - h)}{dh} = \frac{1}{2AC}\left[-C + \frac{1}{2\sqrt{\Delta(r_E - h)}}(2C(A(1-B) - (r_E - h)C) - 4AC)\right]$$

Where $\Delta(r_E - h) = [A(1-B) - (r_E - h)C^2] + 4AC(r_E - h)$ is the discriminant of the high energy range expression.

The expressions of the transmission probability and its derivative remain the same as eq. 6 and 10 respectively. However, the values of p and q are changed, following the expressions given by Kobetich & Katz [11]:

$$q = 0.0059\, Z^{0.98} + 1.1$$

$$p = 1.8\,(\log_{10} Z)^{-1} + 0.31$$

This dose expression should only be considered valid above 10 keV, as it is the domain of validity of the range energy relationship (eq. 5b) used in this case. The dose profiles resulting from the high energy model are shown in figure 6. They are compared with MicroElec and our low energy model based on eq. 5a in the example of Cu.

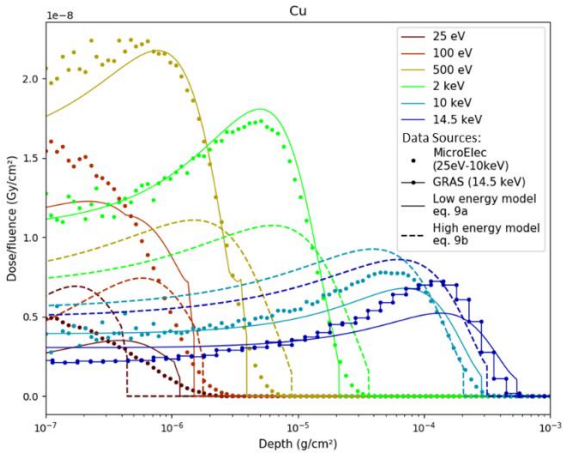

Figure 6: Comparison of the low energy and high energy analytical models

At 10 keV, the maximum difference between the high energy analytical model and MicroElec is 40%, and the shapes of the dose profiles are similar. However, the maximum error for the low energy dose model is 20%, thus it can still be considered acceptable.

At 14.5keV, which corresponds to the limit of validity of the low energy model, it underestimates the peak of the dose with an error of 40%. However, the dose deposited near the surface is still more accurate with the low energy model. Indeed, the high energy model is based on the first assumption of eq. 11 which does not consider the backscattering process.

For the energies below 10 keV, the dose given by MicroElec is significantly underestimated by the high energy model, and the improvements brought by the low energy model are clearly visible.

Finally, the dose profiles given by this work's model for the rest of the materials are provided in Appendix II. The analytical formulation of the deposited energy is in relatively good agreement with the Monte Carlo simulations for most materials.

The agreement is less satisfactory for lower energies, which can be linked to the limitations of the models used. Indeed, the error increases on average to 50% at 50 eV and below, up to a factor 2 in worst cases. This is due to the fact that the transport of electrons at very low energies becomes a random-motion walk due to the predominance of the elastic interactions. When an inelastic interaction happens, the electron deposits all its energy on a single point and comes to rest. As a result, the amount of energy deposited between h and h+dh cannot be approximated by a continuous energy loss anymore, which can explain the discrepancies between the model and the simulation at 50 eV and below. For the same reason, the dose-depth profiles have been validated for depths above a few angströms only. Indeed, a depth of a few angstroms becomes very close to the atomic distances and the notion of a deposited dose in a volume becomes questionable in both the analytical model and the Monte-Carlo simulations. The quantity of backscattered electrons and the energy they can deposit

near the surface may also vary with the incident energy.

Nevertheless, the average error decreases to 30% at 100 eV. At 250 eV and above, the error for all materials is about 15% on average, and always less than 30%. Consequently, despite the approximations of the model, we can still consider that the agreement with the simulations is satisfactory above 50 eV, and the shape of the dose-depth profiles are generally well reproduced. At 50 eV and below, the model reaches its limits, but still gives a correct reproduction of the depth reached by the very low energy electrons and the dose is estimated within the right order of magnitude, as can be seen in Appendix II.

5 Conclusion

In this work, we have first validated the Monte-Carlo code MicroElec for 3 new materials, namely Fe, Au and Be. Simulations of the dose-depth profiles of electrons have then been performed for 11 monoatomic materials (Be, C, Al, Si, Ti, Fe, Ni, Cu, Ge, Ag, W). Analytical expressions of the dose-depth profiles of electrons have been proposed, based on the analytical expressions for the transmission probabilities and extrapolated ranges of electrons (valid from 10 eV to 14.5 keV) from our previous work [17]. As the code MicroElec is valid for the modeling of the transport of low energy electrons and secondary electron emission, the simulation results have been used to calibrate these new dose expressions. MicroElec was chosen since its validity for electrons spans from the eV to the MeV, which is a definite improvement over the standard GEANT4 models for low energy electrons, which are only valid down to 250eV.

The proposed dose model is based on the energy loss process of electrons in matter and follows a physical approach. It depends on the atomic number and on the parameters F and G from the range-energy relationship that are specific for each material. Since the model is given per incident electron, corrections have been introduced to simulate the elastically and inelastically backscattered electrons. These are respectively the backscattered electron yield of the material, and the computation of the energy deposited by the electrons traveling back to the surface corrected by a retrodiffusion factor. This also allows the model to better reproduce the dose-depth profiles and give a better estimation of the surface dose induced by the inelastically backscattered electrons. The accuracy of the model has been checked with MicroElec and other Monte-Carlo simulations for 11 materials. The model is less accurate at 50 eV and below, and some discrepancies can be observed depending on the energy or the material, but on the whole the dose-depth profiles are faithfully reproduced by the model. The agreement with the reference data from MicroElec is acceptable (error less than 30% above 100 eV), as well as the one with the other Monte-Carlo codes (Walker, OSMOSEE, GRAS) above 1keV. This low energy analytical model is also a definite improvement over the high energy model below 10 keV. As a conclusion, and taking into account all these elements, the validity of the dose model proposed in this work can be considered to span from about 10-20eV to 14.5keV with a satisfactory agreement with our Monte-Carlo code in this range of energies.

This analytical model allows the estimation of the dose deposited close to the surface of a material by low energy electrons (<keV). As the ionizing energy released by incident electrons in irradiated materials is dissipated in the form of secondary electrons, this kind of formula can be used to develop simple expressions of secondary emission yield models. The proportion of electrons (ionizing dose) produced close to the surface of the solid and escaping from the material can be estimated by combining the presented dose analytical expression with both the range/energy and the transmission rate function described in this work. This approach

of SEY modelling will be presented in a future work.

Acknowledgements

The authors would like to thank ONERA, CNES and CEA for providing the financial support for this work.

References

[1] C. Inguimbert, P. Caron, Q. Gibaru, A. Sicard, N. Balcon, R. Ecoffet, Surface ionizing dose for space applications estimated with low energy spectra going down to hundreds of eV, IEEE Transactions on Nuclear Science. (2020) 1–1. https://doi.org/10.1109/TNS.2020.3045200.

[2] K. Ohmi, Beam-Photoelectron Interactions in Positron Storage Rings, Phys. Rev. Lett. 75 (1995) 1526–1529. https://doi.org/10.1103/PhysRevLett.75.1526.

[3] N. Balcon, D. Payan, M. Belhaj, T. Tondu, V. Inguimbert, Secondary Electron Emission on Space Materials: Evaluation of the Total Secondary Electron Yield From Surface Potential Measurements, IEEE Transactions on Plasma Science. 40 (2012) 282–290. https://doi.org/10.1109/TPS.2011.2172636.

[4] J. Puech, E. Sorolla, J. Sombrin, M. Belhaj, P. Mader, J. Sinigaglia, Multipactor effect within RF dielectric components, Mulcopim. (2017).

[5] N. Fil, M. Belhaj, J. Hillairet, J. Puech, Multipactor threshold sensitivity to total electron emission yield in small gap waveguide structure and TEEY models accuracy, Physics of Plasmas. 23 (2016) 123118. https://doi.org/10.1063/1.4972571.

[6] G.F. Dionne, Effects of secondary electron scattering on secondary emission yield curves, Journal of Applied Physics. 44 (1973) 5361–5364. https://doi.org/10.1063/1.1662156.

[7] G.F. Dionne, Origin of secondary-electron-emission yield-curve parameters, Journal of Applied Physics. 46 (1975) 3347–3351. https://doi.org/10.1063/1.322061.

[8] A. Plaçais, M. Belhaj, J. Hillairet, J. Puech, A three-dimensional Dionne model for multipactor simulations, Physics of Plasmas. 27 (2020) 053512. https://doi.org/10.1063/5.0004076.

[9] K.-H. Weber, Eine einfache reichweite-energie-beziehung für elektronen im energiebereich von 3 keV bis 3 MeV, Nuclear Instruments and Methods. 25 (1963) 261–264. https://doi.org/10.1016/0029-554X(63)90196-4.

[10] E.J. Kobetich, R. Katz, Energy Deposition by Electron Beams and Delta Rays, Phys. Rev. 170 (1968) 391–396. https://doi.org/10.1103/PhysRev.170.391.

[11] E.J. Kobetich, R. Katz, Electron energy dissipation, Nuclear Instruments and Methods. 71 (1969) 226–230. https://doi.org/10.1016/0029-554X(69)90019-6.

[12] J. Cazaux, A new model of dependence of secondary electron emission yield on primary electron energy for application to polymers, J. Phys. D: Appl. Phys. 38 (2005) 2433–2441. https://doi.org/10.1088/0022-3727/38/14/020.

[13] N. Bundaleski, M. Belhaj, T. Gineste, O.M.N.D. Teodoro, Calculation of the angular dependence of the total electron yield, Vacuum. 122 (2015) 255–259. https://doi.org/10.1016/j.vacuum.2015.04.010.

[14] S. Clerc, J.R. Dennison, R. Hoffmann, J. Abbott, On the Computation of Secondary Electron Emission Models, IEEE Transactions on Plasma Science. 34 (2006) 2219–2225. https://doi.org/10.1109/TPS.2006.883379.

[15] H. Seiler, Secondary electron emission in the scanning electron microscope, Journal of Applied Physics. 54 (1983) R1–R18. https://doi.org/10.1063/1.332840.

[16] Y. Lin, D.C. Joy, A new examination of secondary electron yield data, Surface and Interface Analysis. 37 (2005) 895–900. https://doi.org/10.1002/sia.2107.

[17] Q. Gibaru, C. Inguimbert, M. Belhaj, M. Raine, D. Lambert, Monte-Carlo simulation and analytical expressions for the extrapolated range and transmission rate of low energy electrons [10 eV–10 keV] in 11 monoatomic materials, Applied Surface Science. 570 (2021) 151154. https://doi.org/10.1016/j.apsusc.2021.151154.

[18] A. Valentin, M. Raine, J.-E. Sauvestre, M. Gaillardin, P. Paillet, Geant4 physics processes for microdosimetry simulation: Very low energy electromagnetic models for electrons in silicon, Nuclear Instruments and Methods in Physics Research Section B: Beam Interactions with Materials and Atoms.

288 (2012) 66–73. https://doi.org/10.1016/j.nimb.2012.07.028.
[19] M. Raine, M. Gaillardin, P. Paillet, Geant4 physics processes for silicon microdosimetry simulation: Improvements and extension of the energy-range validity up to 10 GeV/nucleon, Nuclear Instruments and Methods in Physics Research Section B: Beam Interactions with Materials and Atoms. 325 (2014) 97–100. https://doi.org/10.1016/j.nimb.2014.01.014.
[20] Q. Gibaru, C. Inguimbert, P. Caron, M. Raine, D. Lambert, J. Puech, Geant4 physics processes for microdosimetry and secondary electron emission simulation: Extension of MicroElec to very low energies and 11 materials (C, Al, Si, Ti, Ni, Cu, Ge, Ag, W, Kapton and SiO2), Nuclear Instruments and Methods in Physics Research Section B: Beam Interactions with Materials and Atoms. 487 (2021) 66–77. https://doi.org/10.1016/j.nimb.2020.11.016.
[21] J. Allison, K. Amako, J. Apostolakis, P. Arce, M. Asai, T. Aso, E. Bagli, A. Bagulya, S. Banerjee, G. Barrand, B.R. Beck, A.G. Bogdanov, D. Brandt, J.M.C. Brown, H. Burkhardt, Ph. Canal, D. Cano-Ott, S. Chauvie, K. Cho, G.A.P. Cirrone, G. Cooperman, M.A. Cortés-Giraldo, G. Cosmo, G. Cuttone, G. Depaola, L. Desorgher, X. Dong, A. Dotti, V.D. Elvira, G. Folger, Z. Francis, A. Galoyan, L. Garnier, M. Gayer, K.L. Genser, V.M. Grichine, S. Guatelli, P. Guèye, P. Gumplinger, A.S. Howard, I. Hřivnáčová, S. Hwang, S. Incerti, A. Ivanchenko, V.N. Ivanchenko, F.W. Jones, S.Y. Jun, P. Kaitaniemi, N. Karakatsanis, M. Karamitros, M. Kelsey, A. Kimura, T. Koi, H. Kurashige, A. Lechner, S.B. Lee, F. Longo, M. Maire, D. Mancusi, A. Mantero, E. Mendoza, B. Morgan, K. Murakami, T. Nikitina, L. Pandola, P. Paprocki, J. Perl, I. Petrović, M.G. Pia, W. Pokorski, J.M. Quesada, M. Raine, M.A. Reis, A. Ribon, A. Ristić Fira, F. Romano, G. Russo, G. Santin, T. Sasaki, D. Sawkey, J.I. Shin, I.I. Strakovsky, A. Taborda, S. Tanaka, B. Tomé, T. Toshito, H.N. Tran, P.R. Truscott, L. Urban, V. Uzhinsky, J.M. Verbeke, M. Verderi, B.L. Wendt, H. Wenzel, D.H. Wright, D.M. Wright, T. Yamashita, J. Yarba, H. Yoshida, Recent developments in Geant4, Nuclear Instruments and Methods in Physics Research Section A: Accelerators, Spectrometers, Detectors and Associated Equipment. 835 (2016) 186–225. https://doi.org/10.1016/j.nima.2016.06.125.
[22] M. Azzolini, M. Angelucci, R. Cimino, R. Larciprete, N.M. Pugno, S. Taioli, M. Dapor, Secondary electron emission and yield spectra of metals from Monte Carlo simulations and experiments, J. Phys.: Condens. Matter. 31 (2018) 055901. https://doi.org/10.1088/1361-648X/aaf363.
[23] J. Pierron, C. inguimbert, M. Belhaj, T. Gineste, J. Puech, Electron emission yield for low energy electrons: Monte Carlo simulation and experimental comparison for Al, Ag, and Si Electron emission yield for low energy electrons: Monte Carlo simulation and experimental comparison for, Journal of Applied Physics. 121 (2017) 215107. https://doi.org/10.1063/1.4984761.
[24] H.-Y. Chang, A. Alvarado, T. Weber, J. Marian, Monte Carlo modeling of low-energy electron-induced secondary electron emission yields in micro-architected boron nitride surfaces, Nuclear Instruments and Methods in Physics Research Section B: Beam Interactions with Materials and Atoms. 454 (2019) 14–22. https://doi.org/10.1016/j.nimb.2019.05.079.
[25] M. Dapor, Secondary electron emission yield calculation performed using two different Monte Carlo strategies, Nuclear Instruments and Methods in Physics Research Section B: Beam Interactions with Materials and Atoms. 269 (2011) 1668–1671. https://doi.org/10.1016/j.nimb.2010.11.029.
[26] K. Ohya, D. Takami, T. Yamanaka, Modeling of charging effect on ion induced secondary electron emission from nanostructured materials, Journal of Vacuum Science & Technology B, Nanotechnology and Microelectronics: Materials, Processing, Measurement, and Phenomena. 29 (2011) 06F901. https://doi.org/10.1116/1.3643752.
[27] C.D. Denton, I. Abril, J.C. Moreno-Marín, S. Heredia-Avalos, R. Garcia-Molina, Energy loss of swift H and He projectiles in Al, Si, Ni and Cu targets, Phys. Stat. Sol. (b). 245 (2008) 1498–1504. https://doi.org/10.1002/pssb.200743283.
[28] B. Da, H. Shinotsuka, H. Yoshikawa, Z.J. Ding, S. Tanuma, Extended Mermin Method for Calculating the Electron Inelastic Mean Free Path, Phys. Rev. Lett. 113 (2014) 063201. https://doi.org/10.1103/PhysRevLett.113.063201.
[29] F. Salvat, A. Jablonski, C.J. Powell, ELSEPA—Dirac partial-wave calculation of elastic scattering of electrons and positrons by atoms, positive ions and molecules, Computer Physics Communications. 165

(2005) 157–190. https://doi.org/10.1016/j.cpc.2004.09.006.
[30] I.M. Bronshtein, B.S. Fraiman, VTORICHNAYA ELEKTRONNAYA EMISSIYA. (Secondary Electron Emission)., 1969, 1969. https://www.osti.gov/biblio/4160985.
[31] D.C. Joy, A database on electron-solid interactions, Scanning. 17 (1995) 270–275. https://doi.org/10.1002/sca.4950170501.
[32] H. Shinotsuka, S. Tanuma, C.J. Powell, D.R. Penn, Calculations of electron stopping powers for 41 elemental solids over the 50eV to 30keV range with the full Penn algorithm, Nuclear Instruments and Methods in Physics Research Section B: Beam Interactions with Materials and Atoms. 270 (2012) 75–92. https://doi.org/10.1016/j.nimb.2011.09.016.
[33] M.J. Berger, J.S. Coursey, M.A. Zucker, J. Chang, Stopping-Power & Range Tables for Electrons, Protons, and Helium Ions, NIST. (2017). https://dx.doi.org/10.18434/T4NC7P.
[34] L. Katz, A.S. Penfold, Range-Energy Relations for Electrons and the Determination of Beta-Ray End-Point Energies by Absorption, Rev. Mod. Phys. 24 (1952) 28–44. https://doi.org/10.1103/RevModPhys.24.28.
[35] C. Feldman, Range of 1-10 kev Electrons in Solids, Phys. Rev. 117 (1960) 455–459. https://doi.org/10.1103/PhysRev.117.455.
[36] B.N. Subba Rao, A simple formula for the transmission and absorption of monoenergetic electrons, Nuclear Instruments and Methods. 44 (1966) 155–156. https://doi.org/10.1016/0029-554X(66)90456-3.
[37] T. Tabata, R. Ito, S. Okabe, Generalized semiempirical equations for the extrapolated range of electrons, Nuclear Instruments and Methods. 103 (1972) 85–91. https://doi.org/10.1016/0029-554X(72)90463-6.
[38] T. Tabata, P. Andreo, K. Shinoda, An analytic formula for the extrapolated range of electrons in condensed materials, Nuclear Instruments and Methods in Physics Research Section B: Beam Interactions with Materials and Atoms. 119 (n.d.) 463–470.
[39] T. Tabata, V. Moskvin, P. Andreo, V. Lazurik, Y. Rogov, Extrapolated ranges of electrons determined from transmission and projected-range straggling curves, Radiation Physics and Chemistry. 64 (2002) 161–167. https://doi.org/10.1016/S0969-806X(01)00469-8.
[40] D. Tan, B. Heaton, Simple empirical relations for electron CSDA range and electron energy loss, Applied Radiation and Isotopes. 45 (1994) 527–528. https://doi.org/10.1016/0969-8043(94)90120-1.
[41] C.G.H. Walker, M.M. El-Gomati, A.M.D. Assa'd, M. Zadražil, The secondary electron emission yield for 24 solid elements excited by primary electrons in the range 250–5000 ev: a theory/experiment comparison, Scanning. 30 (2008) 365–380. https://doi.org/10.1002/sca.20124.
[42] J. Pierron, C. Inguimbert, M. Belhaj, M. Raine, J. Puech, Ionizing Dose Calculations for Low Energy Electrons in Silicon and Aluminum, IEEE Transactions on Nuclear Science. 64 (2017) 2340–2348. https://doi.org/10.1109/TNS.2017.2662220.
[43] G. Santin, V. Ivanchenko, H. Evans, P. Nieminen, E. Daly, GRAS: a general-purpose 3-D Modular Simulation tool for space environment effects analysis, IEEE Transactions on Nuclear Science. 52 (2005) 2294–2299. https://doi.org/10.1109/TNS.2005.860749.

Appendix I: Parameters of the range and transmission rate model

In this section, the expressions of the range and transmission rate model from ref. [17] are reminded.

The parameters F and G are specific to each material and given in Table A1 in ref. [17].

The practical range $r(E)$ is defined by:

$$R_0(E) = \begin{cases} D(E+E_r)^F : 10eV < E \leq 14.5keV \\ AE\left[1 - \dfrac{B}{(1+CE)}\right] : E \geq 14.5keV \end{cases}$$

With the following parameters:

$R_{0,Al} = 3 \cdot 10^{-7}\ g/cm^2$ is the extrapolated range of 50 eV electrons in aluminum obtained from the MicroElec simulations,

$E_0 = 14.5\ keV$
$A = (1.06 \cdot Z^{-0.38} + 0.18) \cdot 10^{-3}\ g/cm^2\,.keV$

$B = 0.22 \cdot Z^{-0.055} + 0.78$
$C = (1.1 \cdot Z^{0.29} + 0.21) \cdot 10^{-3}\ g/cm^2\,.keV$

$$E_r = \frac{E_0}{\left(\dfrac{AE_0\left[1 - \dfrac{B}{(1+CE_0)}\right]}{G \cdot R_{0,Al}} - 1\right)^{\frac{1}{F}}}$$

$$D = \frac{AE_0\left[1 - \dfrac{B}{(1+CE_0)}\right]}{(E_0+E_r)^F}$$

The transmission rate is given for an energy E in MeV as:

$$\eta(E,h) = e^{-(qh/R_0(E))^p}$$

$$R_0(E) = D(E+E_r)^F,$$

$$\begin{cases} E \geq 2\ \text{keV} : p = 1.1 + 1.772\ e^{(-0.04Z)^{2/3}} \\ \qquad\qquad q = -0.0022\ \text{Z} + 1.6 \\ E < 2\ \text{keV} : p = \dfrac{\left(1.772\ e^{(-0.04Z)^{2/3}} - 0.12\right)}{2\ \text{keV}} E + 1.6 \\ \qquad\qquad q = -0.0022\ \text{Z} + 1.44 \end{cases}$$

Appendix II: Comparison between the analytical model and the Monte-Carlo simulations for the 11 materials

In this section, the dose profiles computed with MicroElec (dots) are compared with the analytical model (solid lines).

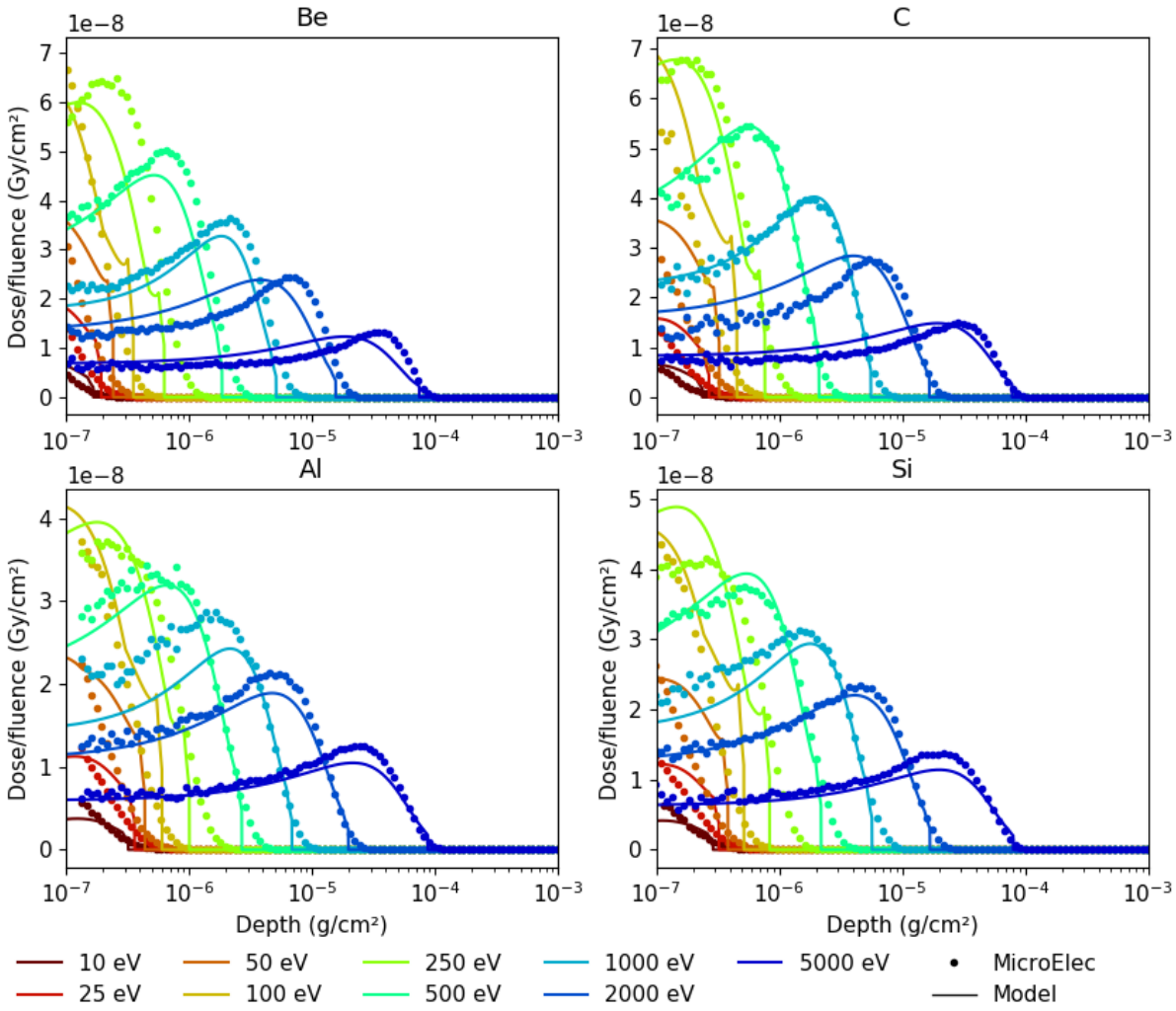

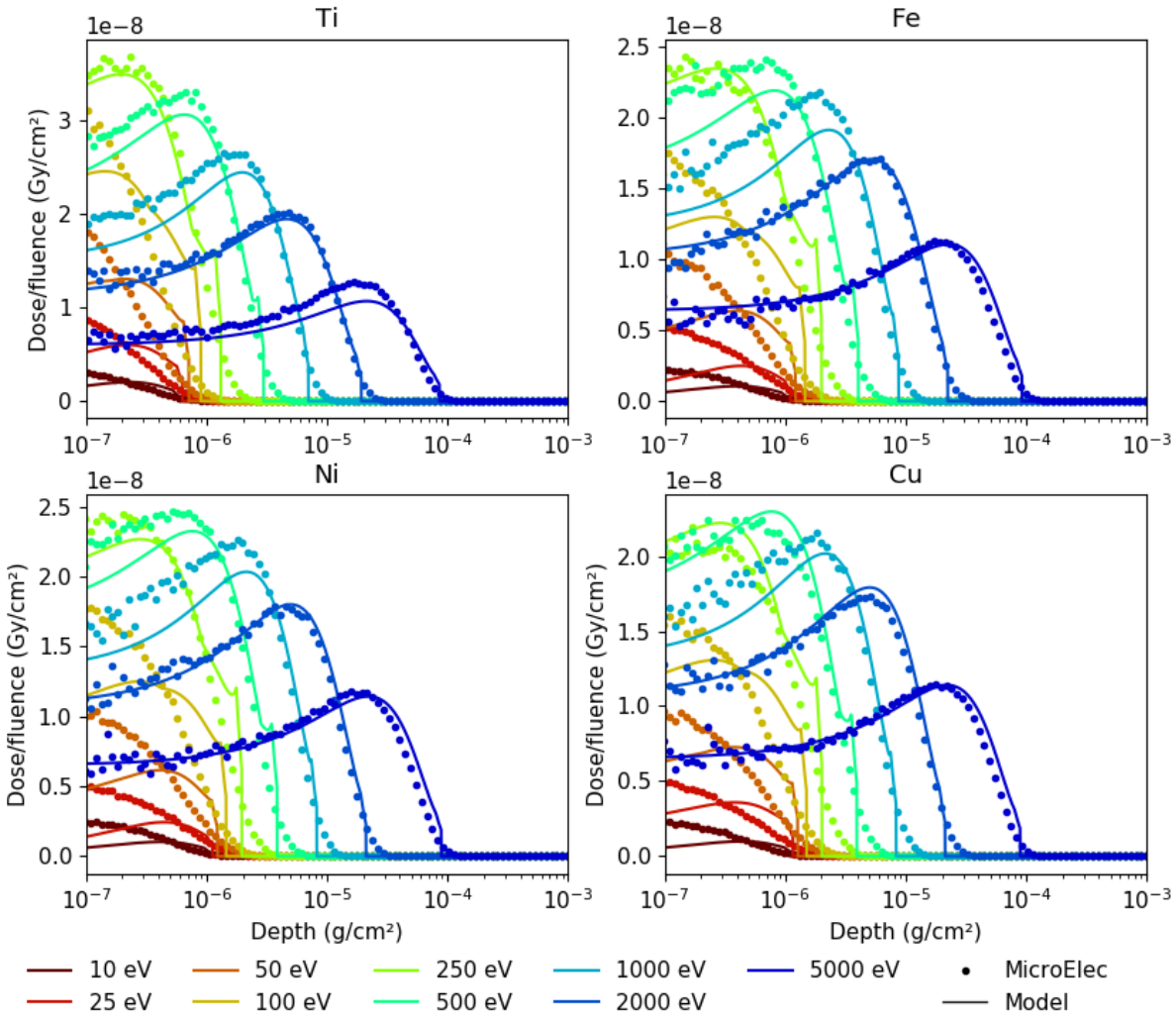
Ti
Fe
Ni
Cu
1e−8
Dose/fluence (Gy/cm²)
Depth (g/cm²)
10 eV
25 eV
50 eV
100 eV
250 eV
500 eV
1000 eV
2000 eV
5000 eV
MicroElec
Model

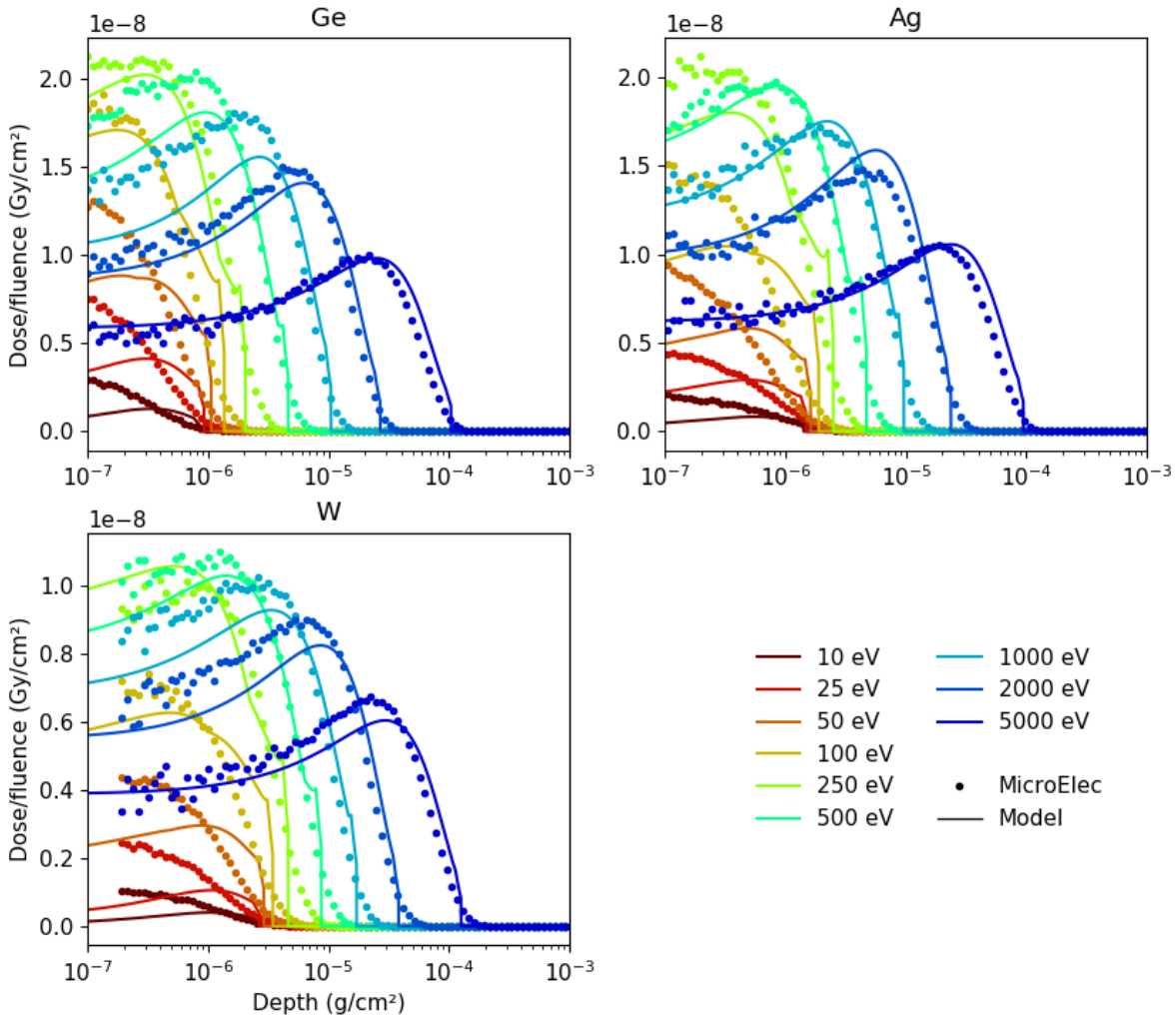
Ge
Ag
W
1e−8
Dose/fluence (Gy/cm²)
Depth (g/cm²)
10 eV
25 eV
50 eV
100 eV
250 eV
500 eV
1000 eV
2000 eV
5000 eV
MicroElec
Model

Appendix III: Comparison of MicroElec and GRAS dose profiles

In this section, the dose profiles computed with MicroElec (dots) are compared with GRAS (lines).

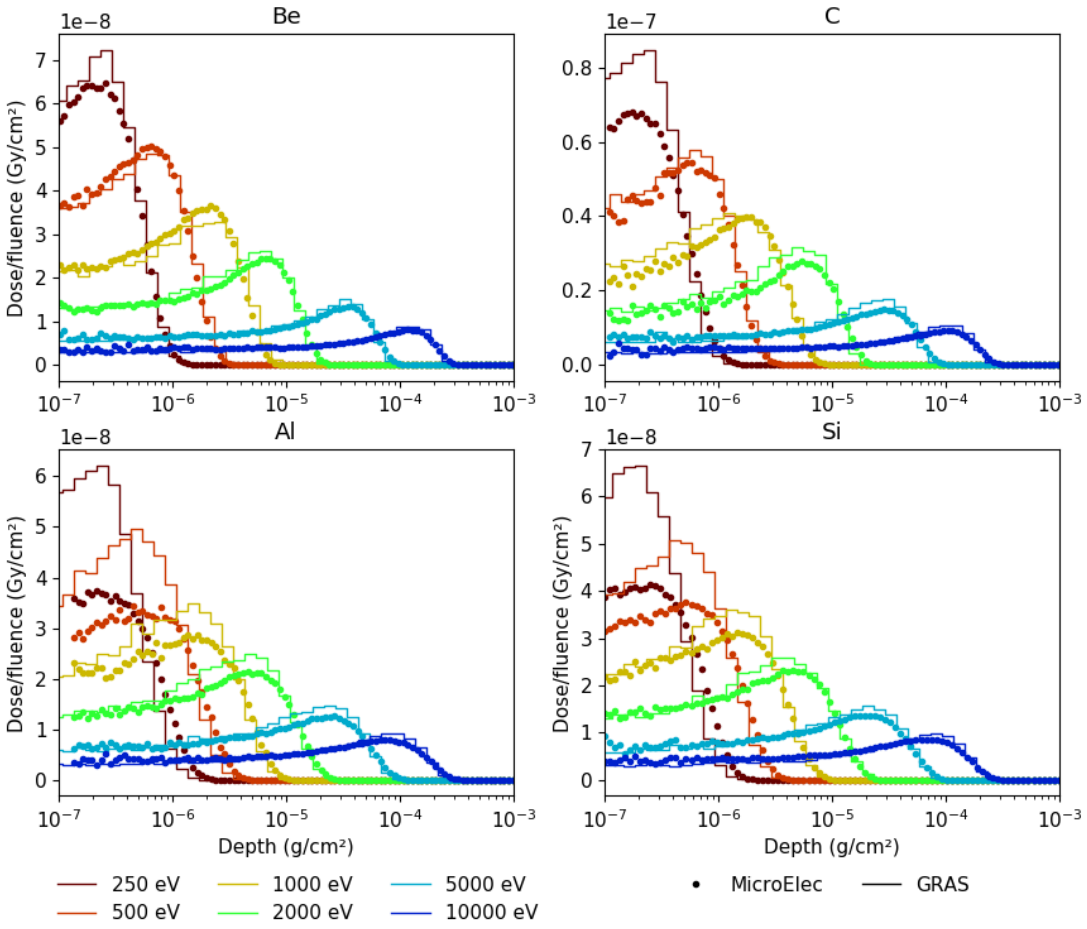

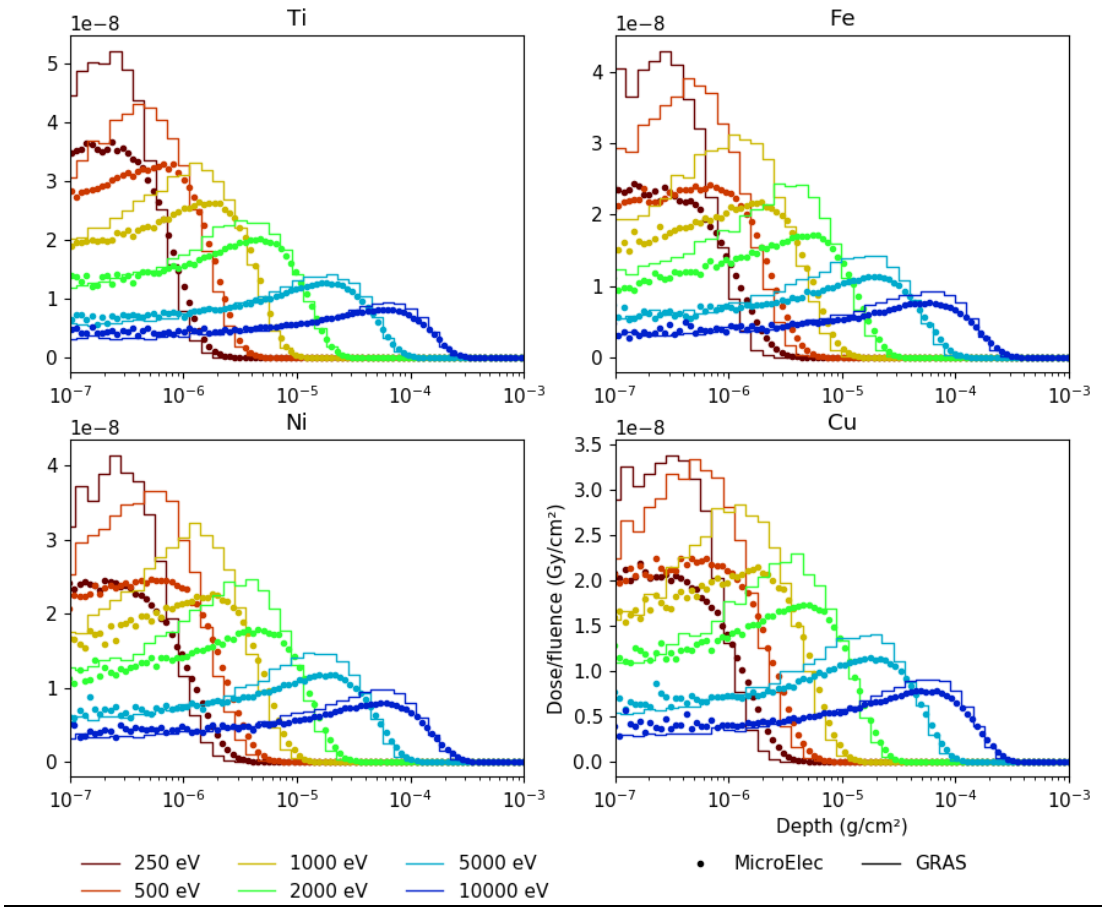
Ti
Fe
Ni
Cu
1e−8
Dose/fluence (Gy/cm²)
Depth (g/cm²)
250 eV
500 eV
1000 eV
2000 eV
5000 eV
10000 eV
MicroElec
GRAS

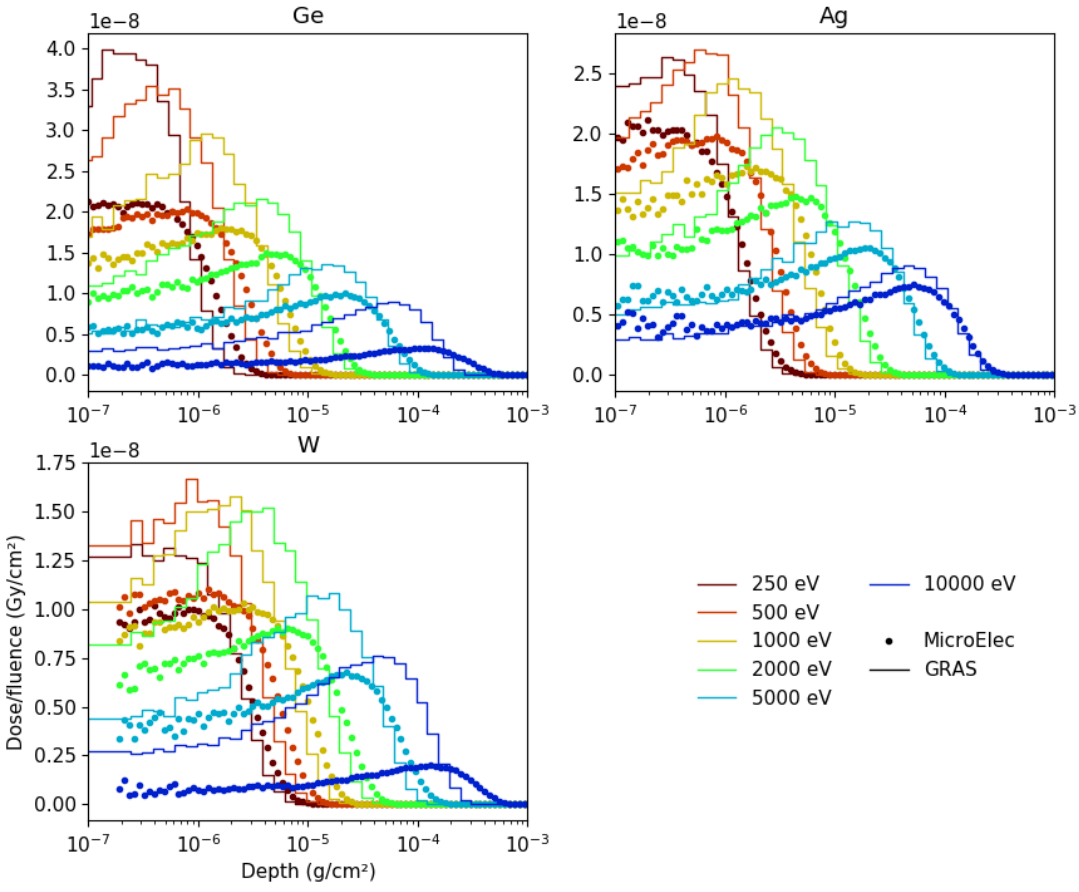
Ge
Ag
W
1e−8
Dose/fluence (Gy/cm²)
Depth (g/cm²)
250 eV
500 eV
1000 eV
2000 eV
5000 eV
10000 eV
MicroElec
GRAS